Measurement Bandwidth Extension Using Multisine Signals: Propagation of Error

Kate A. Remley, *Senior Member, IEEE*, Dylan F. Williams, *Fellow, IEEE*, Dominique Schreurs, *Senior Member, IEEE*, and Maciej Myslinski

***Abstract*—We describe a post-processing technique that extends the effective measurement bandwidth of narrowband vector receivers by phase aligning overlapping measurements. We study the repeatability of the method and the propagation of errors as increasing numbers of bands are stitched together. The method can be used to find phase errors both in the excitation band of frequencies, as well as in distortion products, for periodic multisine signals.**

***Index Terms*—Broadband wireless communications, digitally modulated signal, large-signal network analyzer (LSNA), multisine signal, phase alignment, phase detrending, relative phase, sampling oscilloscope, vector signal analyzer (VSA).**

I. Introduction

ONE TECHNIQUE for extending the useful measurement bandwidth of vector receivers is based on "stitching" together a series of overlapping frequency bands using the overlapping tones for phase alignment. A well-known issue with stitching methods is that phase errors in the measurement increase as more bands are stitched together unless an external reference signal is used. When an external reference signal is not used, measurement errors depend on the characteristics of the receiver, including its sensitivity and phase measurement accuracy. These quantities may, in turn, depend on characteristics of the measured signal, such as its peak-to-average-power ratio, the rise and fall times of transitions, and random noise introduced during transmission. To understand the interaction of these factors, we study the propagation of error as bands are stitched together in the context of a stitching method based on phase detrending of multisine signals.

Stitching methods are used to extend the measurement bandwidth of vector receivers such as vector signal analyzers (VSAs) [1], large-signal network analyzers (LSNAs) [2], and real-time spectrum analyzers [3].[1] These vector receivers maintain the phase relationships between measured frequency components using methods such as real-time sampling or sampling downconversion. Accurate measurement of the phase components of signals and distortion products is critical for characterization of telecommunication systems that use complex modulation schemes, as well as for development and verification of measurement-based behavioral models of electronic circuits and systems [4]–[6].

The measurement bandwidths of commercially available instruments have increased from around 10 MHz only a few years ago to over 100 MHz today. However, even more bandwidth is needed for a complete vector characterization of distortion products several hundred megahertz from the carrier. This is necessary, for example, in measurements of broadband wireless signals at millimeter-wave frequencies.

Full-bandwidth instruments such as digital sampling oscilloscopes [7], [8] offer broadband capability and may be fully calibrated, but typically do not offer the dynamic range of narrowband vector receivers. Consequently, development of bandwidth extension methods that maintain phase relationships between measured frequency components using high dynamic-range instruments has been the subject of a great deal of research.

One class of methods that has been proposed for measuring the phases of frequency components in broadband scenarios is based on the use of an alignment signal whose characteristics are known or assumed *a priori*. Examples may be found in [9]–[13]. These methods are generally restricted to measurement of simple signals such as two- or three-tone signals and their distortion products, or are limited in measurement bandwidth by vector signal generators or receivers.

LSNAs based on sampling downconversion, but modified for broadband measurements, have been proposed in [14]–[16]. These modified instruments are not currently available commercially, although the necessary modifications are described in the references. A commercially available VNA-based instrument is described in [17]. The instruments of [14], [16], and [17] utilize a comb generator with a narrow frequency spacing as a phase reference, providing a known alignment signal that enables the measurement of signals that are more complex than those of [9]–[13]. The instrument of [15] adds a switch to allow the samplers to step through the envelope of a broadband modulated signal. In addition to requiring specialized hardware, the instruments of [14]–[17] may not provide the frequency resolution of an instrument such as a VSA, which can have resolution bandwidths comparable to a spectrum analyzer in the kilohertz or hertz range.

A second class of bandwidth extension method [18], [19] is not hardware based. These methods stitch together sequentially

Manuscript received June 30, 2009; revised November 18, 2009. First published January 22, 2010; current version published February 12, 2010.

K. A. Remley and D. F. Williams are with the National Institute of Standards and Technology, Boulder, CO 80305 USA (e-mail: remley@boulder.nist.gov; dylan@boulder.nist.gov).

D. Schreurs and M. Myslinski are with ESAT-Telemic, Katholieke Universiteit Leuven (K.U. Leuven), Leuven 3001, Belgium (e-mail: Dominique.Schreurs@esat.kuleuven.be; maciej.myslinski@esat.kuleuven.be).

Color versions of one or more of the figures in this paper are available online at http://ieeexplore.ieee.org.

Digital Object Identifier 10.1109/TMTT.2009.2038655

[1]Commercial products are identified solely for completeness of description; such identification does not constitute an endorsement by the National Institute of Standards and Technology (NIST). Other products may work as well or better.

measured frequency bands that are offset in center frequency by up to half of the measurement bandwidth. Overlapping frequency components of a periodic signal are aligned by maximizing a cross-correlation function [18] or minimizing an error function [19]. Subsampling may be used to optimize the alignment between measured samples. One advantage of these techniques is that they do not require the use of additional hardware or instrumentation.

The stitching technique discussed here is similar to the methods of [18] and [19] in that overlapping measurement bands are joined together by aligning individual measurements. The method described here uses an efficient alignment procedure based on minimization of an analytic error function operating on only the phase components of the measured signal. Alignment may be carried out using as few as two overlapping frequency components and is not restricted to sampled time steps.

This method is particularly well suited for use with multisine excitations [6], [7], [15], [16], [20]–[24], where a test signal is engineered to have a certain peak-to-average-power ratio by specifying certain phase relationships. The use of multisines also allows us to easily study the propagation of errors in the method as the number of stitched bands increases because the magnitude and phase of each frequency component can be readily specified. The difference between the measured and specified phases then provides a simple metric for studying the errors in stitching methods.

Our bandwidth extension method is described in Section II, and measurement results for a two-port circuit are described in Section III. We study the propagation of error in Section IV, including the sensitivity of the method to phase measurement errors as a function of the peak-to-average-power ratio of the signal, the number of overlapping frequency components, and the severity of the initial measured phase error. We also compare the repeatability of the method to that from measurements made with a calibrated sampling oscilloscope.

II. Bandwidth Extension Based on Phase Alignment

The bandwidth extension method described here, like those described in [18] and [19], aligns overlapping frequency bands of sequential measurements to achieve bandwidths several times wider than that of the narrowband vector receiver itself. In our multisine-based method, measurements are collected that overlap in frequency by a minimum of two tones in order to phase align adjacent bands [24]. These measurements do not need to be collected simultaneously, although collecting them within a reasonably short period will minimize instrumentation drift.

We first determine a reference time t_{ref} that minimizes the difference between a set of "target" phase values (for example, phase values provided by the user to the signal generator) and those that were measured, shown by "M1" in Fig. 1. Determination of a reference time is necessary because the relative phase relationships between frequency components depend on where the signal is sampled within the envelope period. We provide an overview of this phase alignment (or "detrending") procedure in the Appendix, and the method is described in detail in [24].

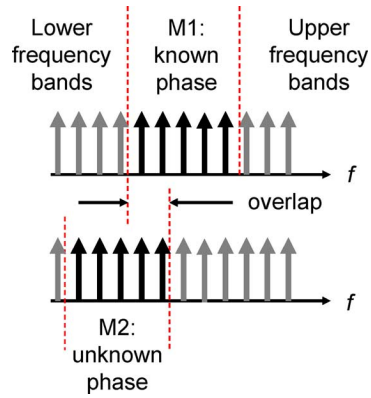

Fig. 1. Illustration of the bandwidth extension method. The phases of the tones in the excitation band are the first to be aligned (shown in the top graph labeled M1). In the second measurement (M2), P overlapping tones are used as targets for phase aligning the lower-adjacent band of frequencies.

The aligned phases in the first measurement band are then used as target values for aligning the phases in the upper and lower adjacent frequency bands, as shown by "M2" in Fig. 1. We continue a sequential process of phase alignment while moving to further adjacent frequency bands until the last band is reached. The user-specified target phases only need to be provided in the first measurement band where the excitation signal is generated. Since we use a common reference time to align all measurements, phase alignment is automatic for frequency components for which there are no targets, such as intermodulation distortion products. This is one of the key strengths of our method.

Mathematically, if the phases of the frequency components in the Mth measured band are given by the vector Φ_M, we use a subset of P_M of these phases at the edge of the measured band as targets for phase alignment in the adjacent $(M+1)$th measured band. An analytic expression provides a rough estimate of the reference time. More precise phase alignment is then carried out by minimizing an error function $E(t)$ that expresses the mean square error in the difference between the known target values in the Mth band and the measured frequency components in the $(M+1)$th band

$$E(t) = \sum_{p'=1}^{P} \left|\theta_{p'}(t) - \theta_{p,\mathrm{target}}\right|^2 \tag{1}$$

where p and p' are the overlapping tones measured in the Mth and $(M+1)$th acquisition (denoted by "overlap" in Fig. 1). We calculate $E(t)$ at time points around the rough initial guess and select as t_{ref} the time that provides the minimum error between the measured and target phase values. By minimizing the error, rather than setting the phase of a measured frequency component to an ideal value [25], our phase alignment procedure provides a realistic picture of the nonidealities of the signal generation and measurement instruments.

For both upper and lower adjacent frequency bands, we carry out $M = 1, \ldots, R_{\mathrm{BW}}$ detrending operations, where R_{BW} is the number of bandwidths to be joined together on either side of the carrier. Note that this method requires initial experiment design such that the measured overlapping components fall on the same frequency values.

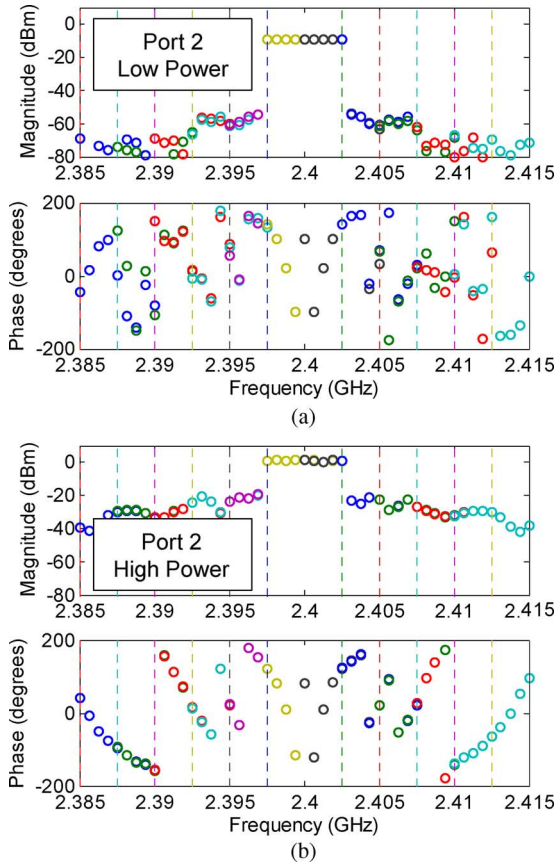

Fig. 2. LSNA measurements of a nine-tone low peak-to-average-power ratio multisine applied to a broadband amplifier. In (a) and (b), the top graph is magnitude and the bottom graph is the detrended phase. (a) Output for a low-power input signal. (b) Output for a high-power input signal. Vertical dashed lines show the center frequency of each measurement. The measured bandwidth is 30 MHz, over four times the bandwidth of the LSNA we used.

III. Two-Port Distortion Measurement

The method described above can be applied to two-port measurements providing that the signals at both ports are sampled simultaneously. We phase align the signals at the output port using the reference time $t_{\rm ref}$ determined from the input port tones for which we have target values. Once the time alignment is carried out, we can characterize the time delay through the system under test and phase align distortion products generated by the system under test as well.

As an example, Fig. 2(a) and (b) shows measurements of the wave variable b_2 at the output port of a broadband amplifier having a gain of approximately 10. Two different excitation power levels are shown: low power (-15 dBm) in Fig. 2(a) and high power ($+5$ dBm) in Fig. 2(b). Eleven LSNA measurements were made: one in the center band and five stitched above and below. The top graph in each figure shows the magnitude and the bottom graph shows the detrended phase. The excitation was a nine-tone Schroeder multisine [20], [23] having a frequency spacing of 500 kHz and a carrier frequency of 2.4 GHz. The relative phases in a Schroeder multisine are designed for a low peak-to-average-power ratio and are defined as

$$\phi_k = \frac{k(k-1)\pi}{S}, \qquad k = 1, 2, \ldots, S \tag{2}$$

where S is the number of tones in the multisine signal and ϕ_k is the phase of the kth tone in radians. Use of low peak-to-average-power ratio multisines allows us to test system distortion under modulated-signal conditions separately from tests of the effects of distortion induced by transient peaks. Other algorithms for low peak-to-average power ratios can be found, for example, in [23], [26].

The vertical dashed lines in Fig. 2 represent the center frequency of each of the ten stitched measurement bands. The excitation band covers a 5-MHz band around the center frequency. These nine tones are the only frequency components for which we have target phase values. To minimize phase dispersion, we used only the inner 4 MHz of the LSNA's 8-MHz measurement bandwidth in the stitching procedure.

The phases shown in the bottom graphs of Fig. 2(a) and (b) were found from a $t_{\rm ref}$ determined by the a_1 excitation signal components. The phases of the b_2 distortion components were found using this $t_{\rm ref}$ as well. As an example of the phase change in the output wave variable when the amplifier was driven into compression, the component of a_1 at the carrier frequency had a measured phase value of -38.6° for both low and high input powers. At the output, this frequency component had a phase value of 141.4° for the lower power and 121.2° for the higher power. This change in phase of the output signal components was relative to the input, not just relative to each other. The ability to measure this system-level phase shift demonstrates the utility of a full vector two-port measurement.

Toward the edges of the measured frequency band, Fig. 2(a) shows that, for the lower input power level, the distortion products are buried in the system measurement noise. As a result, the magnitudes and phases measured in adjacent bands do not overlay well. At higher power levels, Fig. 2(b) shows that the distortion products have significant energy, and a distinct structure is discernable for both magnitude and phase outside the excitation band of frequencies.

IV. Propagation of Error

Errors in stitching methods that use measured data for phase alignment, rather than an alignment signal, are affected by the characteristics of the measured signals, as well as by the number of overlapping tones used. A signal with a high peak-to-average-power ratio can introduce distortion into both the measurement instrument and the system under test, making the phase detrending procedure less accurate. Noise in the received signal may also introduce errors. Measurement errors in one band will propagate through to subsequent bands, and the severity of phase measurement errors in the initial band of frequencies can affect the outcome in a nonlinear manner. In this section, we study these effects as increasing number of bands are stitched together. Even though the absolute value of the errors in other measurement scenarios and using other stitching methods will be different from those reported here, this study provides the user with information on the interaction of these effects and their relative importance.

A. Measurement Comparison

We compare measurements of a wideband multisine made using a reference instrument to those made using a

stitched-VSA measurement procedure. Our reference measurement is made with a digital sampling oscilloscope having a 20-GHz acquisition bandwidth. The measurement comparison described in [7] gives us sufficient confidence to use the oscilloscope as a broadband reference measurement instrument. For our comparison, we made 50 repeat measurements on both the oscilloscope and the VSA because it was determined in [7] that the mean and standard deviation of 50 measurements converged to a steady-state value in the measurement of similar multisines.

The oscilloscope's time-base distortion was corrected using the method of [8]. The data were then transformed to the frequency domain and the phases were detrended using all of the tones in the multisine as targets. Thus aligned, the measured waveforms were averaged in the time domain to reduce the measurement noise floor, as described in [7].

The VSA was automated to acquire five 20-MHz-wide bands that were subsequently stitched together. The experiment was designed with five overlapping tones. In the discussion that follows, we compare the propagation of error when two, three, or all five of these overlapping tones were used as targets in the phase alignment procedure. Use of two targets is desirable because it allows coverage of a broader frequency range with the fewest stitched bands, but using five targets provides the most data for stitching.

We acquired 12 801 points in each measured band giving a resolution bandwidth of just over 1.56 kHz. The experiment was designed to minimize spectral leakage by setting the acquisition time window to a multiple of the envelope period $1/\Delta f$ where Δf is the spacing between tones in the multisine, as described in [27]. We extracted the frequency components corresponding to the multisine frequencies and carried out the phase alignment/stitching procedure described in Section II.

B. Peak-to-Average-Power Ratio

Because stitching is carried out using measured data, distortion caused by signals having higher peak-to-average-power ratios may affect the ability of the receiver to accurately measure the phase. This will, in turn, affect the ability of the stitching method to align overlapping signals. To study this effect, we again utilized a low peak-to-average-power ratio Schroeder multisine. We compared this to a more realistic multisine signal with a probability density function designed to mimic a 64-QAM digitally modulated signal using the method of [6], [28]. The peak-to-average-power ratio for the 64-QAM-like multisine was approximately 10 dB. Both multisines were 80-MHz wide and consisted of 33 tones, giving a tone spacing of $\Delta f = 2.5$ MHz. A vector signal generator was used to produce the signals with a carrier frequency of 1 GHz. We connected our receivers to the output port through a coaxial cable.

Fig. 3(a) and (b) shows the spectra of the oscilloscope-measured Schroeder and 64-QAM-like signals, respectively. We see a small amount of second-harmonic distortion, as well as intermodulation distortion near the passband of the signals. These effects were studied previously [7] and are due to the signal generator used.

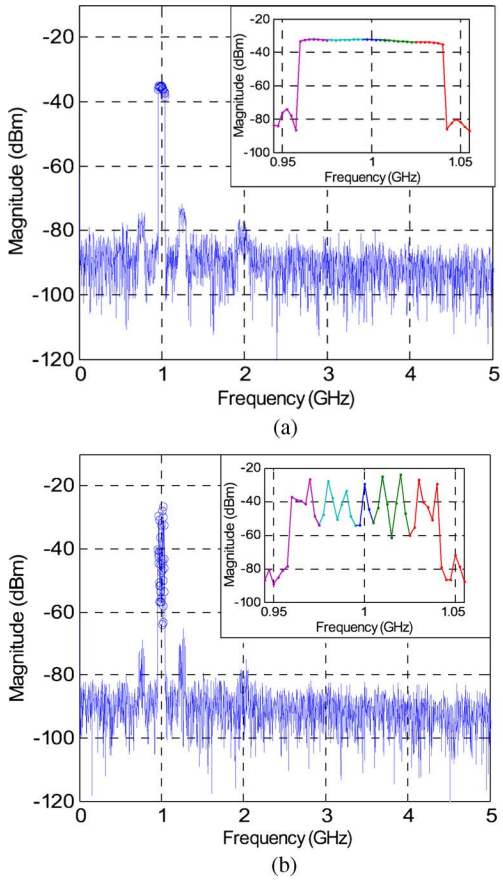

Fig. 3. Spectra of two 80-MHz-wide 33-tone multisine signals measured using a digital sampling oscilloscope. (a) Schroeder multisine. (b) 64-QAM-like multisine. The inset shows the 100-MHz spectrum around the 1-GHz carrier frequency.

Fig. 4 shows the difference between the specified and measured phases (denoted "Phase Error") for the low peak-to-average-power ratio Schroeder multisine [see Fig. 4(a)] and the 64-QAM-like multisine [see Fig. 4(b)] measured by the oscilloscope and VSA. For the latter, five bands containing 13 tones each were stitched together using three target phases; 50 measurements are shown. Note that this phase error quantifies the phase distortion introduced by the system under test (in this case, the signal generator) and is the quantity of interest for this measurement. We see that both receivers report phase errors on the order of 20° at the edges of the 80-MHz passband of the signal, which is consistent with the results of [7] for this signal generator.

The curve labeled "Difference" in Fig. 4(a) and (b) denotes the measurement phase error in the stitching method when the oscilloscope is used as the reference receiver. This value increases toward the edges of the measurement, as expected.

Fig. 4(b) shows that the spread around the mean of the 50 oscilloscope measurements is broader at some frequencies than at others. This is because some of the frequency components in the 64-QAM-like signal were of lower amplitude than others, and these lower amplitude components were affected by the dynamic range of the oscilloscope. In practice, we would typically average all 50 time-domain waveforms from the oscilloscope to reduce this effect.

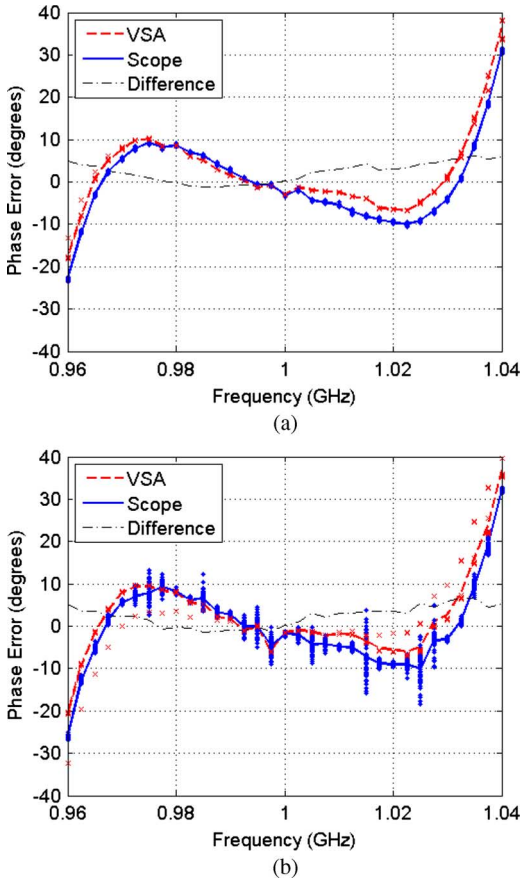

Fig. 4. Thick lines show the mean of 50 repeat measurements of the phase error in the: (a) Schroeder and (b) 64-QAM-like multisines measured by the oscilloscope (solid) and the stitched-VSA procedure (dashed). Individual measurements are shown by dots (oscilloscope) and ×'s (VSA). The difference between the two, the phase measurement error in the stitching method, is shown by the thin dashed–dotted line. Three target phases were used in stitching.

C. Number of Overlapping Tones and Repeatability

A greater number of overlapping tones used in the stitching method means that more target values will be used in the phase detrending procedure. Fig. 5 shows the difference between the oscilloscope and the stitched-VSA measurements for the mean of 50 measurements (shown by the thin line labeled "Difference" in Fig. 4). We see that this difference is less than 8° at the edges of the passband when two, three, or five targets were used in the phase alignment/stitching process. This represents the maximum measured error in the stitched-VSA method for this measurement, significantly less than the measured quantity of interest, which was the phase error in the signal generator itself. The difference was less than 8° for the 64-QAM-like multisine as well, as indicated in Fig. 4(b).

The asymmetry in the difference curves occurs because we used initial-guess targets that were not centered at the carrier frequency. The signal generator we used can have significant carrier leakthrough, and thus, we avoid the use of the carrier in the initial analytic solution.

The number of target phases used in the phase alignment procedure did not have a significant effect on the difference between the mean value of the VSA measurement and the oscilloscope measurement of the phase error in the vector signal generator.

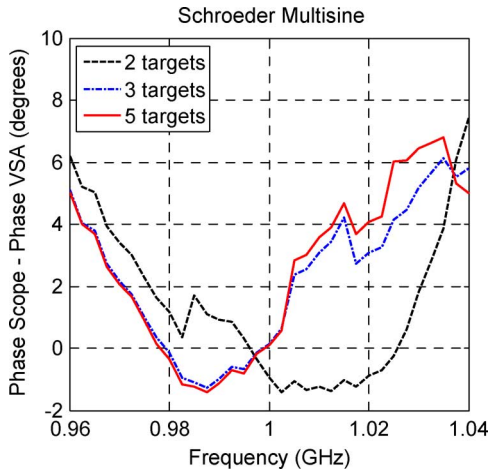

Fig. 5. Difference between the mean of 50 oscilloscope measurements and 50 stitched-VSA measurements for different numbers of target phase values. The Schroeder multisine is shown, although the results were comparable for the 64-QAM-like signal.

However, the number of target phases does have an effect on the standard deviation of the repeat measurements. We calculate the standard deviation in the measurement of the jth frequency component x_j as

$$s_{x_j} = \sqrt{\frac{1}{N-1}\sum_{i=1}^{N}(x_{i,j} - \overline{x}_j)^2} \tag{3}$$

where $x_{i,j}$ is the ith measured value of the jth frequency component, $\overline{x}_j$ is the mean over all measurements of that frequency component, and $N = 50$ measurements were made.

Fig. 6(a) and (b) shows the standard deviation for 50 repeat measurements for different numbers of targets. Each repeat is the difference between the specified and the measured phase. The lowest standard deviation occurs when five targets are used, covering almost half of the stitched frequency band. The use of fewer targets enables the use of fewer measured frequency bands, although it results in an increased standard deviation.

Fig. 6(b) also shows that standard deviation in the oscilloscope measurements is highest for tones in the 64-QAM-like multisine that have lower amplitudes, as mentioned above. We do not see a corresponding increase in the standard deviation of the stitched-VSA measurements since each measurement uses the full dynamic range of the instrument.

Fig. 6(a) and (b) shows that the value of the standard deviation in the stitched VSA measurements increases further from the center frequency. This increase is approximately linear within a given measurement band and the increase is smaller when greater numbers of tones are used as targets. This variability can be caused by, for example, phase measurement errors in the receiver, or additive noise in the transmitted signal, as discussed in Section IV-D.

D. Measurement Errors and Additive Noise

To study the effects of additive-noise-based phase errors on the method as increasing numbers of bands are stitched together, we conducted a Monte Carlo simulation where Gaussian-distributed noise was introduced into the phase of

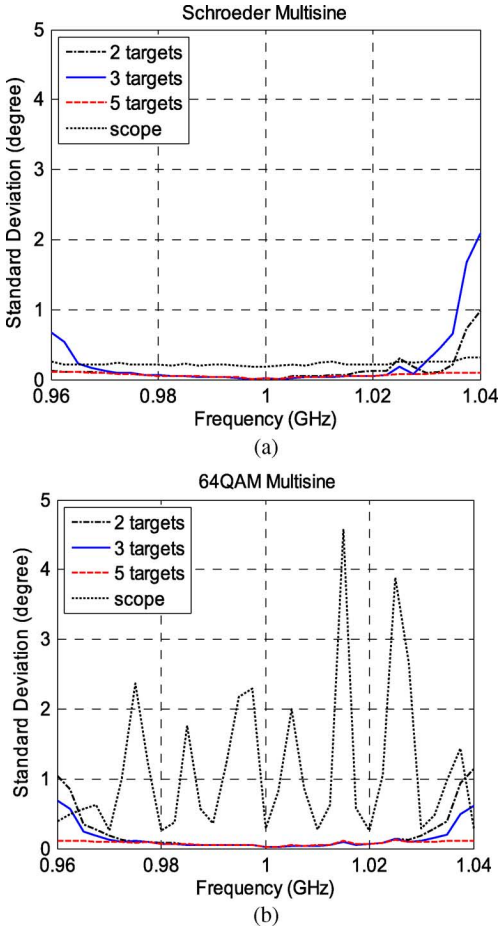

Fig. 6. Standard deviation in 50 oscilloscope (light dotted line) and stitched-VSA (dashed and solid lines) measurements of the signal generator's phase error in: (a) the Schroeder multisine and (b) the 64-QAM-like multisine. Different numbers of targets were used in the phase-alignment procedure, as noted. The peaks in the standard deviation in (b) correspond to the lower signal levels shown in the inset of Fig. 3(b).

each frequency component in the multisine excitation. In this study, the phase alignment procedure had to "overcome" a given level of phase distortion in the form of additive noise during the stitching process. This additive noise could represent a random process introduced by the vector receiver such as its noise floor when weak signals are received, or random noise introduced on the signal during transmission. Our unperturbed data was one set of the stitched-VSA measurement data for the 64-QAM multisine. We study the difference in phase error for small and large values of additive noise relative to the input signal.

1) Small Errors: We first used a value of simulated additive noise representative of a real laboratory-based measurement. For this, we used the maximum standard deviation of the 50 measurements discussed in Section IV-C. Since this measurement setup consisted of a signal generator connected directly to a signal analyzer, the variance between measurements was internally generated by the instrumentation. From an examination of the data in Section IV-C, the standard deviation of our raw measurements was never greater than 0.15° for any of the 13 frequency components in the five frequency bands for the 50 repeat measurements we made using five targets. We

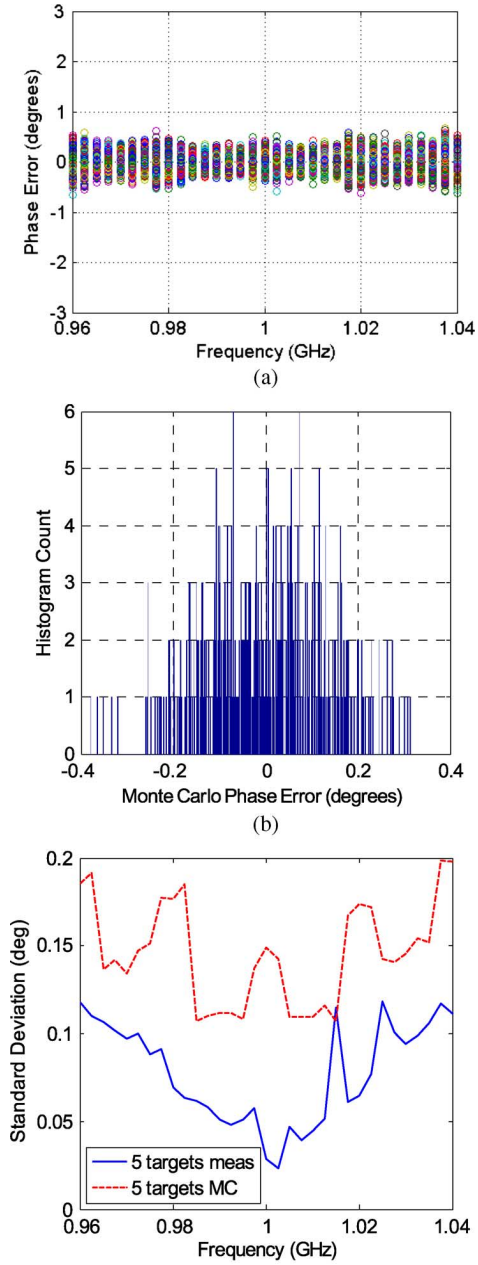

Fig. 7. (a) Difference between measurement and 500 Monte Carlo simulations where Gaussian-distributed noise with a standard deviation of 0.15° was introduced into each frequency component before stitching. (b) Distribution of phase error at 970 MHz. (c) Standard deviation of measured and simulated phase errors.

conducted 500 Monte Carlo simulations using this standard deviation.

Fig. 7(a) shows the difference between the unperturbed phases and the Monte Carlo simulations when five target phases were used in the stitching procedure. The repeatability of the stitching procedure is less than 1° for this level of additive noise. Fig. 7(b) shows the distribution of phases at the frequency of 970 MHz, essentially a vertical slice in the graph of Fig. 7(a). Here we see an approximately Gaussian-distributed phase difference between the unperturbed and perturbed simulated phases. This is expected because we used Gaussian-distributed additive noise in the simulations.

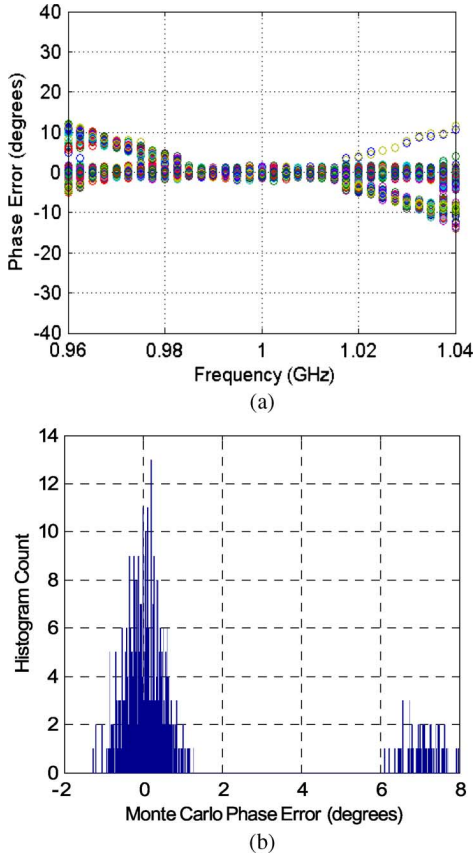

Fig. 8. (a) Difference between measurement and 500 Monte Carlo simulations where Gaussian-distributed noise with a standard deviation of 0.5° was introduced into each frequency component before stitching. (b) Distribution of phase error at 970 MHz. Five target phases were used.

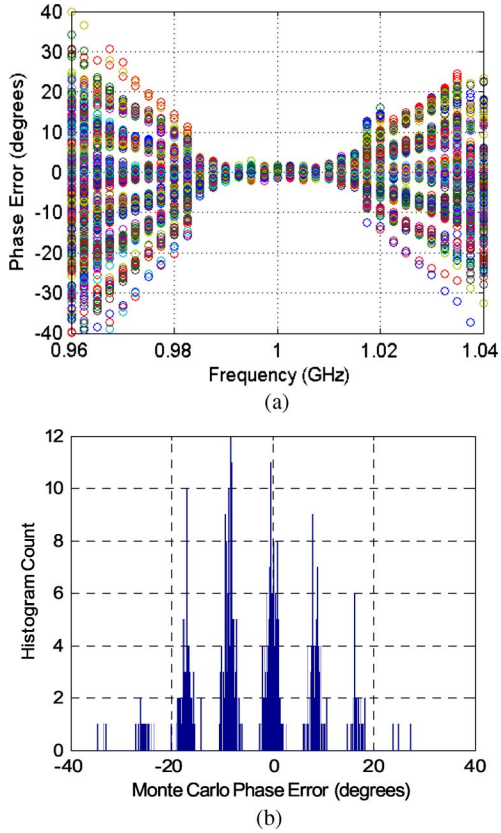

Fig. 9. (a) Difference between measurement and 500 Monte Carlo simulations where Gaussian-distributed noise with a standard deviation of 0.5° was introduced into each frequency component before stitching. (b) Distribution of phase error at 970 MHz. Two target phases were used.

In Fig. 7(c), we compare the standard deviation in the phase error from the 50 measurements [also shown in Fig. 6(b)] to that of the Monte Carlo simulations. We used the maximum standard deviation at any frequency over all of our measurements as the standard deviation in our Monte Carlo simulation. As a result, the Monte Carlo simulation displays a higher overall standard deviation than do the measurements. However, the order-of-magnitude agreement between the two indicates that the Monte Carlo simulation approximates the measurement well for a standard deviation close to that of the measurements.

2) Large Errors: We next used the Monte Carlo simulations to predict how errors propagate in the stitching method for larger values of phase error. We again carried out 500 Monte Carlo simulations of the 64-QAM-like multisine. As before, 13 frequency components were included in each stitched band, and five bands were stitched together. The standard deviation in the Gaussian-distributed noise was 0.5°, larger than noise that would be introduced by most instrumentation, but this value of additive noise is certainly possible for measurements made in the field.

Figs. 8 and 9 show the difference between the unperturbed phases and the Monte Carlo simulations (top graphs) and the distribution of phases at 970 MHz (bottom graphs) when five target phases were used (Fig. 8) and when two target phases were used (Fig. 9).

We again see approximately Gaussian-distributed phase errors, but in both cases the errors are sometimes spaced around an offset phase value. This offset in phase is regularly spaced and increases linearly away from the center 13-tone band of frequencies. The value of the offset is an integer multiple of approximately 7° at 970 MHz.

The source of the regularly spaced clusters of phase solutions can be traced to the error function, given in (1), used in the phase alignment procedure. The stitching procedure solution finds the global minimum of the error function. However, the error function contains many local minima, one corresponding to each cycle of the carrier frequency. If the phase error is large enough, the algorithm may converge to an adjacent local minimum, resulting in the clustering of errors seen in Figs. 8 and 9. The number of local minima is related to the envelope period by

$$N_{\text{minima}} = \frac{f_c}{\Delta f}. \tag{4}$$

Here, $f_c = 1$ GHz and $\Delta f = 2.5$ MHz, and thus, there are 400 cycles of the carrier in each envelope period, and 400 local minima in the error function. Fig. 10 shows a plot of the local minima for the unperturbed 64-QAM-like multisine when two and five target phases are used. Two complete envelope cycles are shown in Fig. 10(a). The close-up view of the global minimum in Fig. 10(b) shows that the broad valley of local minima for the two-target case can lead to a bad choice of global minimum when noise is introduced into the stitched frequency com-

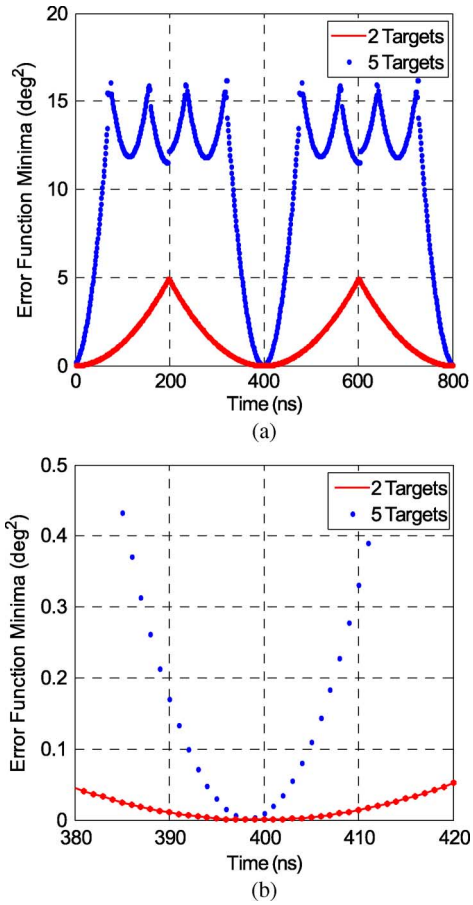

Fig. 10. Plot of the minima of the error function for each RF cycle in the envelope period for the 33-tone 64-QAM-like multisine. (a) Two envelope cycles. (b) Close-up around the global minimum.

ponents. The steeper slope in the five-target case makes it more immune to additive noise.

The clustering of phase errors shown in Figs. 8(a) and 9(a) corresponds to the selection of the wrong global minimum. To confirm this, we estimate the phase offset represented by each local minimum. Each local minimum represents one 360° phase change of the carrier frequency f_c, but some other value of phase change for other frequencies f. We can find this phase difference from

$$\Delta\theta = 360^\circ \left(\frac{f}{f_c} - 1 \right). \tag{5}$$

For a frequency of 970 MHz, (5) gives a phase offset of approximately 11°, close to the offset in the clusters seen in Figs. 8(b) and 9(b). The offset is not exact because the increase in offset is not linear within the center band of frequencies, as can be seen in Figs. 8(a) and 9(a).

Results of this study indicate that when a high level of additive noise or random measurement error is expected in a measurement scenario, the user would be advised to use a larger number of overlapping tones for the stitching procedure. Note that overcoming this random component of measurement error is separate from the method's ability to find systematic phase errors, such as the 20° phase error introduced by the vector signal generator in the examples of Fig. 4.

V. Conclusion

We described a method for extending the measurement bandwidth of vector receivers while maintaining the phase relationships between frequency components. The method presented here enables measurement of wideband signals using narrowband receivers, providing a higher dynamic range than many wideband receivers. The bandwidth extension involves phase alignment of adjacent frequency bands by using overlapping tones as target phases. We demonstrated the use of the method in finding the phase of distortion products at the output port of an amplifier relative to the input port phases over a bandwidth more than four times that of our LSNA. We also used the method to characterize the phase error in a multisine signal generated by a vector signal generator over a frequency band more than three times broader than that of a VSA.

For the signals we studied, the peak-to-average-power ratio had little effect on errors in the stitching method. A study of the number of targets used in the phase alignment procedure showed that, while the error in the method remains relatively constant when two, three, or five overlapping tones are used as targets, the standard deviation of the measurements decreases with an increasing number of targets.

Monte Carlo simulations were used to model the effects of additive noise on the stitched VSA measurements. These simulations helped to illustrate how errors propagate when both small and large values of additive-noise-based phase errors are encountered. We saw that the use of an error function that minimizes the mean-square error between known target phases and measured phases, while computationally efficient, can also lead to clustering in the calculation of phase error for a measured signal when the phase errors are large. This example demonstrated that when the additive noise is expected to be large, the user may wish to use a larger number of target phases.

Our study of propagation of errors in stitching methods that use measured signals for phase alignment provides an understanding on the relative importance of various parameters. We illustrated how these parameters interact with each other in typical measurement scenarios.

Appendix
Phase Alignment

The measured relative phase between frequency components of a periodic signal is a function of the time during the signal's envelope period when it was sampled. Time delays introduced into a measurement by cables, random instrument sampling times (including jitter), and other effects can make it difficult to compare the measured phases with the ones specified by the user unless alignment is carried out.

This effect is illustrated in Fig. 11, where we see a three-component multisine signal that was specified to have a 0° relative-phase offset between its frequency components. As shown in Fig. 11 and discussed in more detail in [24], at the instant the signal is generated ($t = t_{\mathrm{ref}}$), the relative phase relationships between the frequency components ideally match those specified by the user. However, if the signal is sampled at a time later in the envelope period, the relative phase relationship between

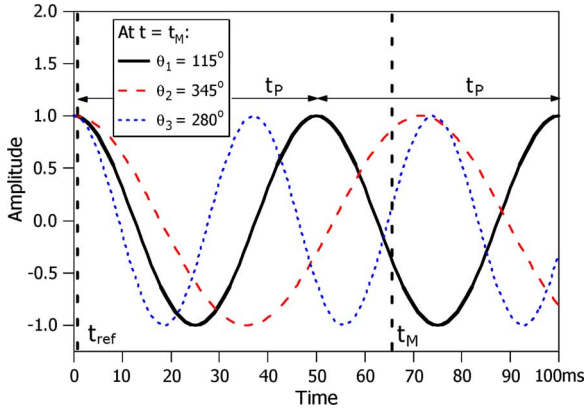

Fig. 11. Illustration of relative phase alignment. At time $t = t_{\rm ref}$, the phase relationships between the three tones are all 0°. The phase relationships are other than 0° when the signal is sampled at a later time (from [24]).

tones can be significantly different from 0°. Even a slight time offset can give the appearance of increased phase distortion in a measurement.

The phase alignment procedure we use [24] first develops an analytic estimate of the difference between $t_{\rm ref}$ and the time $t_{\rm M}$. If the signal generator and receiver were perfect, this analytic expression would give $t_{\rm ref}$ exactly. However, systematic errors in signal generators, analyzers, and random errors such as jitter and drift mean that the analytic estimate needs to be refined. This is done by minimizing an error function that expresses the mean-square error between the known target values and the corresponding measured frequency components. Rather than assuming the signal emitted from the signal generator is perfect, the minimization procedure accounts for the nonidealities of the signal generation and measurement processes as well.

All sampled frequency components in the measurement bandwidth may be phase aligned to the reference time. This includes frequency components for which no target phase values exist such as distortion products, harmonics, and measurements at the second port of a nonlinear two-port device.

ACKNOWLEDGMENT

The authors acknowledge P. Hale, National Institute of Standards and Technology (NIST), Boulder, CO, for assistance with the oscilloscope measurements and calibrations.

REFERENCES

[1] "Agilent vector signal analysis basics," Agilent Technol., Santa Clara, CA, Appl. Note 150-15, Jul. 2004.

[2] T. Van den Broeck and J. Verspecht, "Calibrated vectorial nonlinear-network analyzers," in *IEEE MTT-S Int. Microw. Symp. Dig.*, Jun. 1994, pp. 1069–1072.

[3] Tektronix, "Fundamentals of real-time spectrum analysis," *Primer*, 2004.

[4] D. Schreurs, "Capabilities of vectorial large-signal measurements to validate RF large-signal device models," in *58th ARFTG Conf. Dig.*, Nov. 2001, pp. 169–174.

[5] D. E. Root, J. Verspecht, D. Sharrit, J. Wood, and A. Cognata, "Broad-band poly-harmonic distortion (PHD) behavioral models from fast automated simulations and large-signal vectorial network measurements," *IEEE Trans. Microw. Theory Tech.*, vol. 53, no. 11, pp. 3656–3664, Nov. 2005.

[6] M. Myslinski, D. Schreurs, B. Nauwelaers, K. A. Remley, and M. D. McKinley, "Large-signal behavioral model of a packaged RF amplifier based on QPSK-like multisine measurements," in *Eur. Gallium Arsenide and Other Semiconduct. Appl. Symp.*, Oct. 2005, pp. 185–188.

[7] K. A. Remley, P. D. Hale, D. I. Bergman, and D. Keenan, "Comparison of multisine measurements from instrumentation capable of nonlinear system characterization," in *66th ARFTG Conf. Dig.*, Dec. 2005, pp. 34–43.

[8] P. D. Hale, C. M. Wang, D. F. Williams, K. A. Remley, and J. Wepman, "Compensation of random and systematic timing errors in sampling oscilloscopes," *IEEE Trans. Instrum. Meas.*, vol. 55, no. 6, pp. 2146–2154, Dec. 2006. (Time-base correction software download available online.) [Online]. Available: http://boulder.nist.gov/div815/HSM_Project/HSMP.htm

[9] J. H. K. Vuolevi, T. Rahkonen, and J. P. A. Manninen, "Measurement technique for characterizing memory effects in RF power amplifiers," *IEEE Trans. Microw. Theory Tech.*, vol. 49, no. 8, pp. 1383–1389, Aug. 2001.

[10] P. Draxler, I. Langmore, T. P. Hung, and P. M. Asbeck, "Time domain characterization of power amplifiers with memory effects," in *IEEE MTT-S Int. Microw. Symp. Dig.*, Jun. 2003, pp. 803–806.

[11] J. Dunsmore and D. Goldberg, "Novel two-tone intermodulation phase measurement for evaluating amplifier memory effects," in *33rd Eur. Microw. Conf. Dig.*, Oct. 2003, pp. 235–238.

[12] J. C. Pedro, J. P. Martins, and P. M. Cabral, "New method for phase characterization of nonlinear distortion products," in *IEEE MTT-S Int. Microw. Symp. Dig.*, Jun. 2005, pp. 971–974.

[13] K. A. Remley, D. Schreurs, D. F. Williams, and J. Wood, "Broadband identification of long-term memory effects," in *IEEE MTT-S Int. Microw. Symp. Dig.*, Jun. 2004, pp. 1739–1742.

[14] J. Verspecht, "The return of the sampling frequency convertor," in *62nd ARFTG Conf. Dig.*, Dec. 2003, pp. 155–164.

[15] W. Van Moer and Y. Rolain, "An improved broadband conversion scheme for the large signal network analyzer," *IEEE Trans. Instrum. Meas.*, vol. 2, no. 58, pp. 483–487, Feb. 2009.

[16] M. El Yaagoubi, G. Neveux, D. Barataud, T. Reveyrand, J.-M. Nebus, F. Verbeyst, F. Gizard, and J. Puech, "Time-domain calibrated measurements of wideband multisines using a large-signal network analyzer," *IEEE Trans. Microw. Theory Tech*, vol. 56, no. 5, pp. 1180–1192, May 2008.

[17] P. Blockley, D. Gunyan, and J. B. Scott, "Mixer-based, vector-corrected, vector signal/network analyzer offering 300 kHz-20 GHz bandwidth and traceable response," in *IEEE MTT-S Int. Microw. Symp. Dig.*, Jun. 2005, pp. 1497–1500.

[18] D. Wisell, D. Rönnow, and P. Händel, "A technique to extend the bandwidth of an RF power amplifier test bed," *IEEE Trans. Instrum. Meas.*, vol. 56, no. 4, pp. 1488–1494, Aug. 2007.

[19] M. El Yaagoubi, G. Neveux, D. Barataud, J. M. Nebus, and J. Verspecht, "Accurate phase measurements of broadband multitone signals using a specific configuration of a large-signal network analyzer," in *IEEE MTT-S Int. Microw. Symp. Dig.*, Jun. 2006, pp. 1448–1451.

[20] K. A. Remley, "Multisine excitation for ACPR measurements," in *IEEE MTT-S Int. Microw. Symp. Dig.*, Jun. 2003, pp. 2141–2144.

[21] N. B. Carvalho, K. A. Remley, D. Schreurs, and K. G. Gard, "Multisine signals for wireless system test and design," *IEEE Microw. Mag.*, vol. 9, no. 3, pp. 122–138, Jun. 2008.

[22] J. C. Pedro and N. B. Carvalho, "On the use of multitone techniques for assessing RF components' intermodulation distortion," *IEEE Trans. Microw. Theory Tech.*, vol. 47, no. 12, pp. 2393–2402, Dec. 1999.

[23] R. Pintelon and J. Schoukens, *System Identification: A Frequency Domain Approach*. New York: Wiley, 2001.

[24] K. A. Remley, D. F. Williams, D. Schreurs, G. Loglio, and A. Cidronali, "Phase detrending for measured multisine signals," in *61st ARFTG Conf. Dig.*, Jun. 2003, pp. 73–83.

[25] P. S. Blockley, J. B. Scott, D. Gunyan, and A. E. Parker, "Noise considerations when determining phase of large-signal microwave measurements," *IEEE Trans. Microw. Theory Tech.*, vol. 54, no. 8, pp. 3182–3190, Aug. 2006.

[26] E. van der Ouderaa, J. Schoukens, and J. Renneboog, "Peak factor minimization using time—Frequency domain swapping algorithm," *IEEE Trans. Instrum. Meas.*, vol. 37, no. 1, pp. 144–147, Jan. 1988.

[27] M. D. McKinley, K. A. Remley, M. Myslinski, and J. S. Kenney, "Eliminating FFT artifacts in vector signal analyzer spectra," *Microw. J.*, vol. 49, no. 10, pp. 156–164, Oct. 2006.

[28] J. C. Pedro and N. B. Carvalho, "Designing band-pass multisine excitations for microwave behavioral model identification," in *IEEE MTT-S Int. Microw. Symp. Dig.*, Jun. 2004, pp. 791–794.

Kate A. Remley (S'92–M'99–SM'06) was born in Ann Arbor, MI. She received the Ph.D. degree in electrical and computer engineering from Oregon State University, Corvallis, in 1999.

From 1983 to 1992, she was a Broadcast Engineer in Eugene, OR, serving as Chief Engineer of an AM/FM broadcast station from 1989 to 1991. In 1999, she joined the Electromagnetics Division, National Institute of Standards and Technology (NIST), Boulder, CO, as an Electronics Engineer. Her research activities include metrology for wireless systems, characterizing the link between nonlinear circuits and system performance, and developing methods for improved radio communications for the public-safety community.

Dr. Remley is currently editor-in-chief of *IEEE Microwave Magazine* and chair of the MTT-11 Technical Committee on Microwave Measurements. She was the recipient of the Department of Commerce Bronze and Silver Medals and an Automatic RF Techniques Group (ARFTG) Best Paper Award.

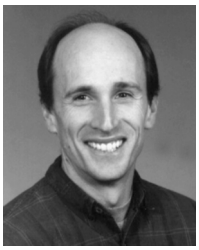

Dylan F. Williams (M'80–SM'90–F'02) received the Ph.D. degree in electrical engineering from the University of California at Berkeley, in 1986.

He joined the Electromagnetic Fields Division, National Institute of Standards and Technology (NIST). Boulder, CO, in 1989. He develops metrology for the characterization of monolithic microwave integrated circuits and electronic interconnects. He has authored or coauthored over 80 technical papers.

Dr. Williams is the editor-in-chief of the IEEE TRANSACTIONS ON MICROWAVE THEORY AND TECHNIQUES. He was the recipient of the Department of Commerce Bronze and Silver Medals, the Electrical Engineering Laboratory's Outstanding Paper Award, two Automatic RF Techniques Group (ARFTG) Best Paper Awards, the ARFTG Automated Measurements Technology Award, and the IEEE Morris E. Leeds Award.

Dominique Schreurs (S'90–M'97–SM'02) received the MSc. and Ph.D. degrees in electronic engineering from the Katholieke Universiteit Leuven (K.U.Leuven), Leuven, Belgium.

She is currently an Associate Professor with K.U.Leuven. She was a Visiting Scientist with Agilent Technologies, ETH Zürich, and the National Institute of Standards and Technology (NIST). Her main research interests concern the (non-)linear characterization and modeling of active microwave and millimeter-wave devices and circuits, and (non-)linear hybrid and integrated circuit design.

Dr. Schreurs serves on the IEEE Microwave Theory and Techniques Society (IEEE MTT-S) Administrative Committee (AdCom). She is vice-chair of the MTT-S TCC. She also serves as education chair on the Executive Committee of the Automatic RF Techniques Group (ARFTG). She was general chair of the 2007 Spring ARFTG Conference and co-chair of the 2008 European Microwave Conference.

Maciej Myslinski was born in Warsaw, Poland, in 1978. He received the Master degree in electronics engineering from the Warsaw University of Technology, Warsaw, Poland, in 2003, and the Ph.D. degree from the Katholieke Univeristeit Leuven (K.U.Leuven), Leuven, Belgium, in 2008.

Since December 2008, he has been a Post-Doctoral Fellow with the ESAT-TELEMIC Research Group, K.U.Leuven. His research interests include practical large-signal measurement-based modeling of high-frequency nonlinear components.

Dr. Myslinski was the recipient of the 2005 Automatic RF Techniques Group (ARFTG) Student Fellowship.